Mechanochemical Synthesis of Nanocrystalline Hydroxyapatite Coating

Ahmed E. Hannora[1*], Alexander S. Mukasyan[2], and Zulkhair A. Mansurov[3]

[1] Faculty of Petroleum and Mining Engineering, Suez Canal University, 43721, Suez, Egypt.
[2] Department of Chemical and Biomolecular Engineering, and Center for Molecularly Engineered Materials University of Notre Dame, 46556, IN, Notre Dame, USA
[3] Institute of Combustion problems, 050012, Almaty, Kazakhstan

Abstract

A novel approach for depositing of hydroxyapatite (HA) films on titanium substrates by using high energy ball milling (HEBM) has been developed. It was demonstrated that a heat treatment of the mechanically coated HA at 800°C for one hour leads to partial transformation of HA phase to β-TCP. It appears that the grain boundary and interface defects formed during MCS reduce this characteristic transformation temperature. Also, it was shown that Ti incorporation into the HA structure causes the lattice shrinkage and reduction of its grain size as compared to pure HA, but also promote the phase transformation of HA to TCP at high temperature. It is important that doping HA by silicon, while also significantly decrease crystallinity of deposited HA layer, results in hindering of the phase transformation process. The Si-doped HA does not show phase transition or decomposition after heat treatment even at 900°C. The samples were investigated by X-ray diffraction, scanning electron microscope, Energy dispersive spectroscopy, Atomic force microscopy, Transmission electron microscopy, inductively coupled plasma (ICP) optical emission spectrometer, Vickers microhardness, Electron paramagnetic resonance.

Introduction

Natural bone is a nanocomposite consisting of mineral fraction, including small apatite crystals and non-stoichiometric calcium phosphate, and organic fraction, which together confer mechanical resistance. In order to simulate the nature bone structure, the synthesis of nanosized hydroxyapatite (HA: $Ca_{10}(PO_4)_6(OH)_2$) has received attention in recent years. Hydroxyapatite (HA: $Ca_{10}(PO_4)_6(OH)_2$) coatings of metallic implants often flake off as a result of poor ceramic/metal interface bonding, which may cause surgery to fail [1]. This problem may be solved by fabrication of metal/HA composites. Some work have been reported on the preparation of Ti-based alloy/HA composite materials or composite coatings for biomedical applications [2-4]. However, most synthetic apatites are formed via high temperature processes, resulting in a well crystallized structure and a large particle size, which show poor biocompatibility. Since kinetic solubility is dependent on particle size, there has been great interest in nanosized HA cement as bone substitute materials [5, 6]. For example, our group has recently described the effect of high energy ball milling (HEBM) on HA and Ti substrate. It was shown that significant decrease of the HA particle and crystalline size as a result of HEBM, leads to the formation of the nano-scale structure. The comparison of surface topography for composite substrates shows that one hour of HEBM with optimum ball to powder ratio equals to 40:1 leads to the reduction of surface particle size from 1.0 μm to 80 nm [7, 8]. Let us discuss these results in more details.

Materials and Methods

Hydroxyapatite powder, Ti-powder (Wako, 99.5%, 250 μm) and 10×8×2 mm Ti-alloy

*corresponding author. Email: Ahannora@yahoo.com

 Printed in Kazakhstan

substrates were used in this work. The powders and/or Ti-substrate were placed into the vibration steel vial (50 Hz) and treated for the different times with optimum ball to powder ratio equals to 40:1. The milling process was carried out without any process control agent. The chamber was sealed in order to prevent contamination from the atmosphere.

As-prepared (coated) samples were annealed in vacuum of 10^{-5} Pa, for one hour, at temperatures ranging between 500°C and 1000°C. All the heat treated samples were then cooled in the furnace. XRD was performed using DRON–6 system. Diffraction measurements were performed using Cu K_α radiation (wavelength λ = 0.15406 nm) with a nickel filter at 25 kV and 25 mA. The diffractometer was operated within range of diffraction angles $20<2\theta<60$ with step-time = 3 seconds and step-size = 0.02 degree.

The microstructural features of the surface layer and coating distribution on substrate surface has been systematically investigated using a Solver PRO scanning probe microscope JSPM-5200, JEOL and scanning electron microscopy Quanta 3D 200i. The sample composition was analyzed by energy dispersive x-ray spectroscopy (EDS) using JEOL JSM-6490 LA analytical SEM. The Electron paramagnetic resonance analysis was done with a JEOL (JES-FA200) ESP conventional X-band spectrometer. A Perkin–Elmer Optima 2000 Dual View inductively coupled plasma (ICP) optical emission spectrometer (USA) was used to carry out the chemical analysis of the used powder especially for Fe and Cr elements. Transmission electron microscopy was performed with JEOL JEM CX at an accelerating voltage of 100 kV.

Results and Discussion

Mechanical milling of Hydroxyapatite powder

The function of HA in all of its applications is largely determined by its morphology, composition, crystal structure, and crystal size distribution. Thus to control the mechanical properties of hydroxyapatite, the influence of such characteristics as particle morphology, particle size distribution and agglomeration have to be studied [9]. It is known that for high energy ball milling process the powder to milling media weight ratio is one of the most important parameter which affects the HA microstructure. Figure 1 shows the XRD of the HEBM-HA powders processed for one hour with different powder/ball weight ratios (W_p:W_b). It can be seen that with increasing W_p:W_b ratio the XRD patterns show a notable broadening and intensity reduction, which indicates the decreasing of crystalline size and powder amoprhization. Increasing of the W_p:W_b ratio to some extent accelerates the rate of amorphization, which is explained by the increase in the kinetic energy of the ball mill charge per unit mass of powders [10, 11]. However, the volume fraction of the amorphous phase in the HEBM powders rises with increasing W_p:W_b ratio, only up to 1:40, while the further increase of the ratio leads to the re-crystallization of HA powder. The latter effect may be related to the too high kinetic energy of the ball mill charge which transformed into heat.

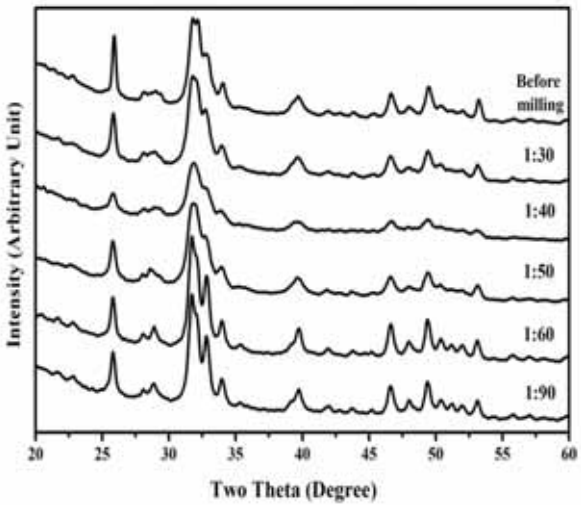

Fig. 1. XRD patterns of HA powder milled one hour for various W_p:W_b ratio.

Using Scherrer equation the unit cell dimensions were calculated for the 1:60 and 1:90 samples, table 1. The slight variation of lattice parameters could be from the accumulated strain through the HEBM process. Since large plastic deformation is induced into the powder particles during mechanical milling, the crystals are strained and the deformation occurs in an inhomogeneous manner. From the XRD data it is also can be concluded that, that decomposition of HA or formation of secondary phases such as tri-calcium phosphate, tetra-calcium phosphate and calcium oxide do not take place throughout the milling process.

Table 1
Unit cell parameters of the mechanical milled HA with Space group P63/m.

Sample	Lattice constant (Å)	Standard Deviation	R_{wp} (%)
Standard card (24-0033)	a = b =9.432 c = 6.881	---------	
1:60 ratio	a = b = 9.443 c = 6.898	0.00141	7.6

Hydroxyapatite powder morphology

Scanning electron microscopy (SEM) and transmission electron microscopy (TEM) was used to analyze the morphology of the as-synthesized powders of hydroxyapatite. As mentioned in the above section, cold welding and fracturing are the two essential processes involved in the HEBM process. Fracture tends to break individual particles into smaller pieces and de-agglomerates particles that have been cold welded. The morphologies of the HA powder particles before ball milling are shown in Fig. 2. It can be seen that HA powder consists of crystallites which have needles and platelets -like morphologies. Higher magnification shows that large HA particles composed of very smaller ones with the size of less than 100 nm. After 1 hour of HEBM (W_p:W_b=1:40) the morphology of the initial large particles significantly changes (Figure 3) due to micro-forging, fracture, agglomeration and de-agglomeration processes. Thin layered (laminated) microstructure dominates in this sample.

However more close inspection by TEM (Figure 4), shows two types morphologies, i.e. needle-like (a) and round shaped (b) could be observed. It is also can be seen that these small particles formed the agglomerates as a result of cold welding phenomenon.

Mechanical, physical and chemical properties of powders may be altered if they are contaminated. The most common contamination in mechanical milling is Fe and Cr elements from the milling tools (vial and balls) since most milling tools are made from those types of elements. The Fe and Cr elements content after one hour of HEBM are shown in Table 2. As the W_b:W_p ratios increases the amount of contamination increases. It is expected that for the lower ratios (10:1) a thin coating of the milling balls by the HA powder is formed which reduces Fe and Cr-contamination. For higher W_b:W_p ratios (60:1) direct collision and friction increases which leads to a significant increase in Fe and Cr contamination.

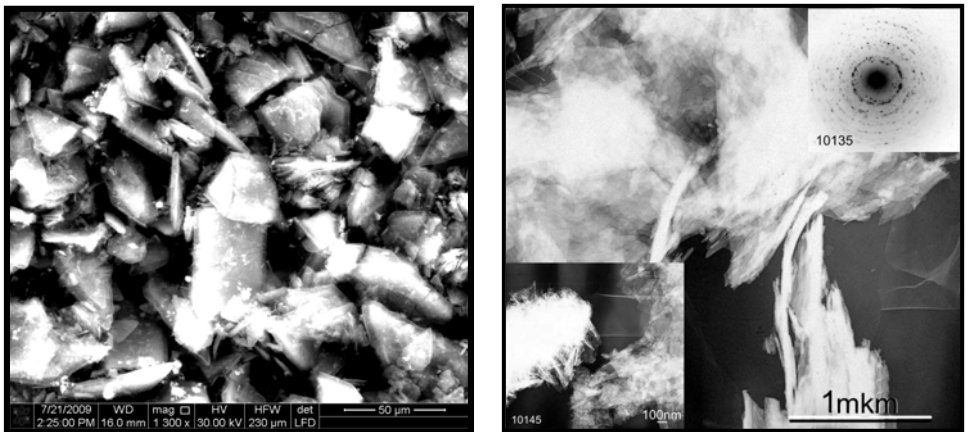

Fig. 2. SEM and TEM needle-like crystallite of HA sample before milling.

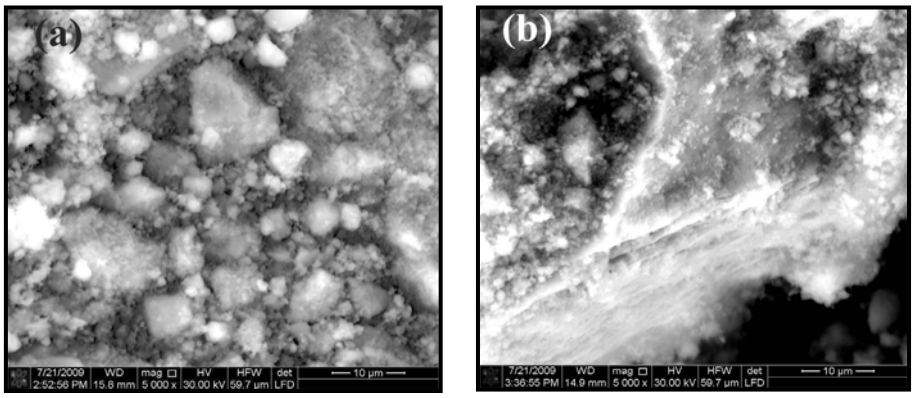

Fig. 3. (a) and (b) Morphologies of HA powder particles after one hour of milling with W_p:W_b=1:40.

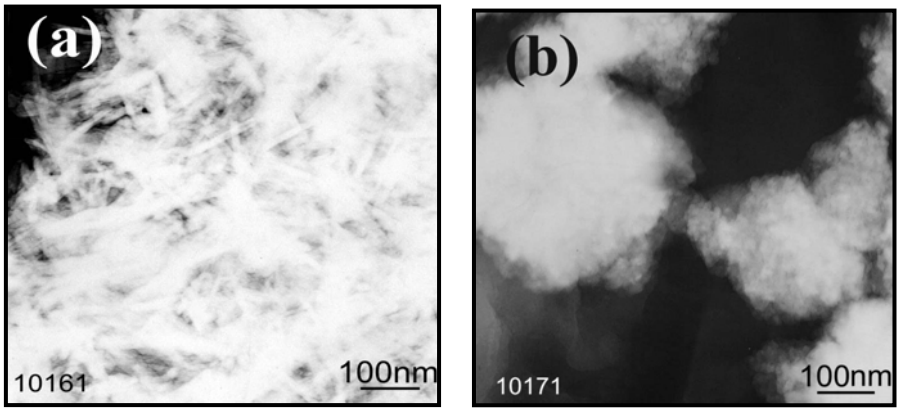

Fig. 4. Hydroxyapatite powder after one hour of milling with W_p:W_b=1:40.

Table 2
Fe and Cr-contamination in one hour milled HA powder.

Elements / W_b:W_p ratios	Fe		Cr	
	ppmw	%	ppmw	%
Before milling	32.3±1.9	0.0032	< 1	$< 10^{-4}$
10:1	302±9	0.03	3.3±0.2	3.3×10^{-4}
30:1	480±14	0.048	6.2±0.3	6.2×10^{-4}
60:1	4787±144	0.479	60±2	6.0×10^{-3}

X-Ray Diffraction of HA coating on Ti-substrate

The XRD patterns shown in Figure 5 illustrate the effect of mechanical treatment on Ti-substrate milled with HA powder. After 1 hour of HEBM the (002) peak which is the most distinct reflection in the XRD pattern for HA shows a notable intensity reduction. The (101) peak of the Ti-substrate only slightly shifted to a higher values, Δd=-0.0024 also (002) and (102) peaks are shifted with Δd=-0.0015 and Δd=-0.0016 respectively.

As reported, [9] the process of covering metallic surfaces with HA at elevated temperatures (*e.g.* plasma-spraying) has a tendency to eliminate the functional group OH in the HA matrix (dehydration) and results in the decomposition of HA into α-tricalcium phosphate, β-tricalcium phosphate and tetracalcium phosphate. Also the condition of high substrate temperature promoted the oxidation of the substrate surface prior to the growth of the HA layer. The oxidation layer degraded the adhesion of the coating to the substrate. As can be concluded from XRD patterns in figure 5, the repeated ball collision with the Ti-substrate resulted in the deposition of HA powder on its surface without any trace of HA decomposition or Ti oxidation.

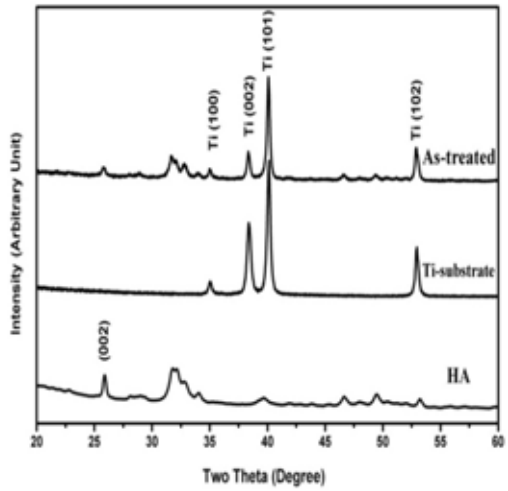

Fig. 5. XRD patterns of ball milled hydroxyapatite coated Ti-substrate after one hour of milling.

Morphology of HA coating on Ti-substrate

Typical morphology of the coated substrate surface is shown in figure 6. It can be seen that after one hour of HEBM, the substrate was covered with HA powder. The inhomogeneous distribution over the entire coated sample could be due to powder particles repeatedly fractured and cold welded on the substrate. The similar result, i.e. inhomogeneous distributed precipitates was observed for calcium and phosphorus ion implanted in a dose of 10^{17} ions/cm^2 [12]. The broad face morphology of the as-coated HA (Figure 6b), implies that the agglomeration of particles occurs due cold welding process. The dome-shaped morphology was also formed in physical-vapor-deposited and laser-deposited HA films [13].

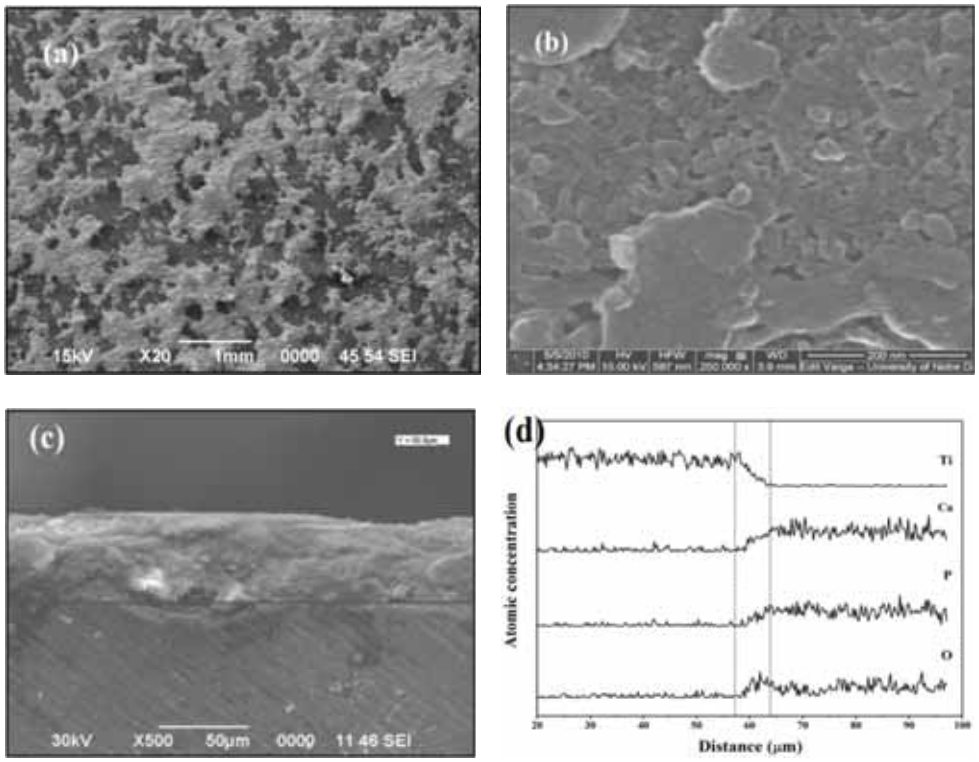

Fig. 6. (a) and (b) Surface morphologies of the as-synthesized HA coating after one hour of milling (c) cross-section microstructure and (d) concentration profile of as-synthesized HA coating

Typical cross-sections of as-treated HA coating shown in Figure 6c where the coating thickness was about 50 µm. The composition of the HA coated sample was analyzed by energy dispersive X-ray spectroscopy (EDS). Figure 6d shows the cross-section microstructure and concentration profile of HA coating produced by mechanical treatment method. Cold welding between particles and substrate under repeated ball collisions led to the formation of a composite coating. HA (Ca, P, O-elements) flowed into the pores between Ti particles under the impact of balls and vice versa. The energy dispersive spectroscopy (EDS) of the as-treated sample, series of point analysis, indicated that the average value of the Ca/P ratio of coated HA was (1.803 ± 0.18) while the stochiometric molar ratio is 1.67 [14].

Atomic force microscopy (AFM) image of the as-coated HA, figure 7 showed that the HA was composed of numerous spherical-shaped aggregates of different sizes. Some spheroids were apparently much larger than others surrounding them. The higher magnification micrograph, figure 7 c,d, revealed that each spheroidal aggregate was comprised of numerous, much smaller units (grains).

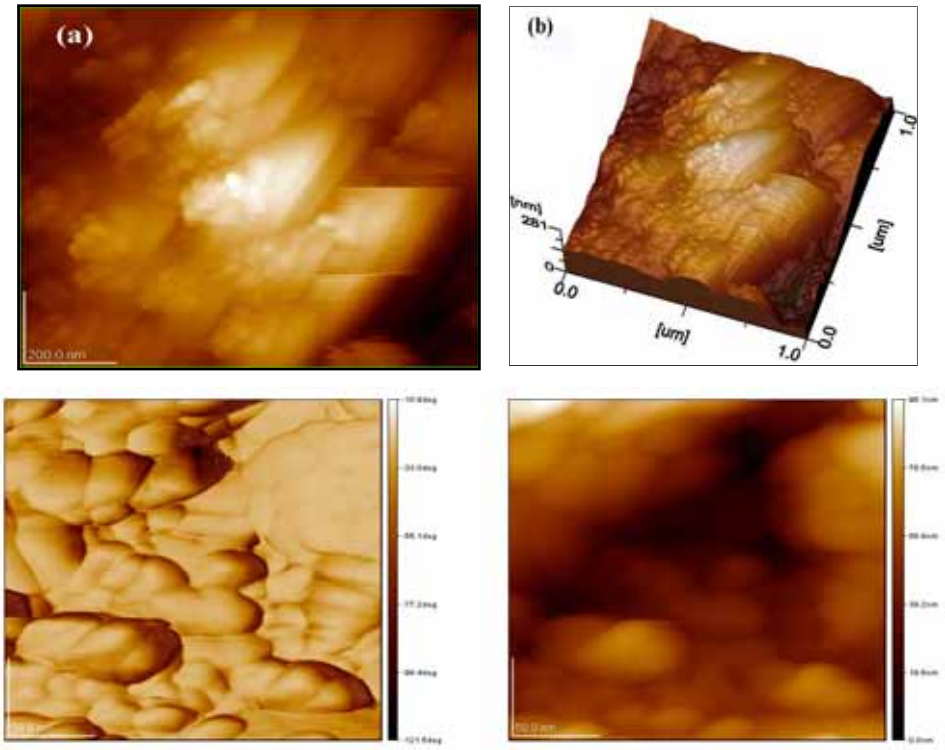

Fig. 7. 2D (a, c, d) and 3D (b) AFM image of the as-coated HA

XRD patterns of deposited HA heated at different temperatures are presented in figure 8. The changes in the XRD patterns give an indication of the influence of temperature on the structure stability of the samples. According to XRD patterns of the coated samples, it is clear that up to 700°C HA phase is stable, i.e. no any phase transition or decompositions were observed. With increasing heat treatment temperature the intensity of HA peaks increases as compared to that of as-treated sample. As the heat treatment temperature is raised to 800°C, the slight decomposition of the HA to $Ca_3(PO_4)_2$ (TCP) can be observed. The amount of TCP increases after 900°C. X-ray peaks of the formed phase were matched to the ICDD (JCPDS) standard, α-tricalcium phosphate (09-0348), β-tricalcium phosphate (03-0690) and titanium oxide (29-1361). This could be due to diffusivity enhancement of Ti in HA matrix and/or effect of MA. It is reported that [15] the HA thermal decomposition occurs in two steps: dehydroxylation and decomposition. Dehydroxylation to oxyhydroxyapatite proceeds at temperatures in the range 850–900°C. The decomposition to TCP and TTCP occurs at temperatures greater than 900°C. Since, both the dehydroxylation and decomposition reactions include water vapor as a product, the rates at which these reactions proceed depend on the partial pressure of H_2O in the furnace. Therefore, the secondary phase formation during sintering could be suppressed by controlling the moisture content in the sintering atmosphere. The high moisture content has the tendency to slow down the decomposition rate by preventing the dehydration of the OH group from the HA matrix. The difference in result in the present work with others could in part be attributed to the difference in humidity in the sintering atmosphere and also to the nature of the deposited material (mechanical treated samples). The transformation from HAP to β-TCP phase occurred at relatively low temperature because of the nano-size nature of HEBM-HAP coating, since fine particles are less stable for heat treatment.

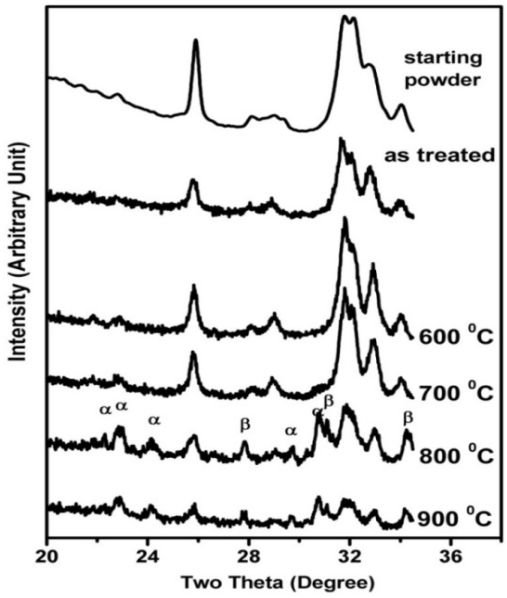

Fig. 8. XRD patterns of HA deposited on Ti-substrate after heated at various temperatures.

According to [16] heat treatment of HA at 800°C for 5h was sufficient for HA to β-TCP transformation. Also, it was shown [17] that for Ti doped samples (100 and 200 ppm of Ti), an endothermic peak, which corresponds to the HA→ β-TCP transformation occurs at 794°C. Note that no reactions were observed in the pure and 50 ppm Ti-doped HA samples. The formation of β-TCP is also a sensitive indicator for Ca/P ratio in HA composition.

Thus the most likely explanation for the existence of β-TCP phase in the heated HEBM-synthesized HA-Ti sample is that the presence of Ti in the incubation media leads to the formation of a calcium-deficient apatite that has a Ca/P ratio less than 1.67. Calcium-deficient HA are less thermally stable than stoichiometric HA. The enhanced diffusivity is believed to be due to the introduction of structural defects such as grain boundaries and interfaces. The correlation between the enhanced diffusivity and the composite microstructure is often reflected by the decrease of reaction temperature with refinement of the composite microstructure. It appears that the interface plays a major role in reducing the reaction temperature. With the reduction of layer thickness and the increase of interface area, the reaction becomes easier. When the reaction becomes easy enough, it can occur during milling, leading to mechanical alloying [18].

Morphology of the annealed HA coating on Ti-substrate

A set of backscattered electron images is shown in figure 9, which illustrate the microstructure evolution of the HA-surface during samples heat treatment. It can be seen that cracks are formed, while no any other microstructural changes can be detected. The presence of the cracks could be due to the difference in coefficients of thermal expansion of HA and Ti-alloy substrate. According to linear elastic fracture mechanics, [19] a constrained film, subjected to stress, would crack when the strain energy released in the process exceeds the energy required to form the crack. Also, cracks could form during cooling of annealed ceramic films deposited on a substrate due to differences between the thermal expansion coefficients of the substrate and the coated film. Finally, MA is an effective way of creating localized plastic deformation, so the cracks formation after heat-treated also could be due to mechanical energy released.

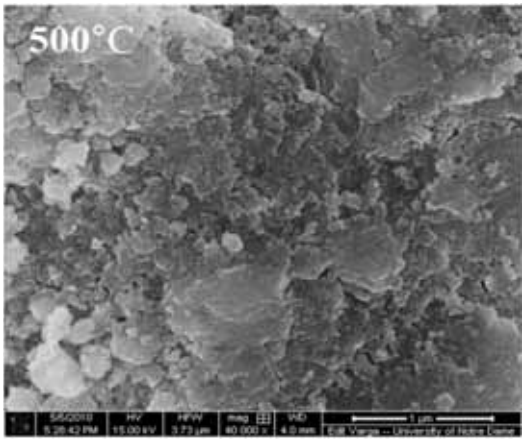

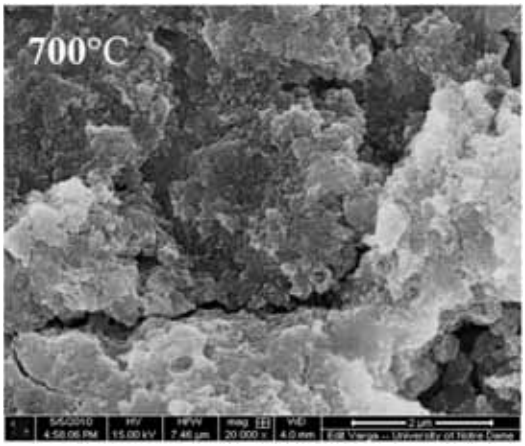

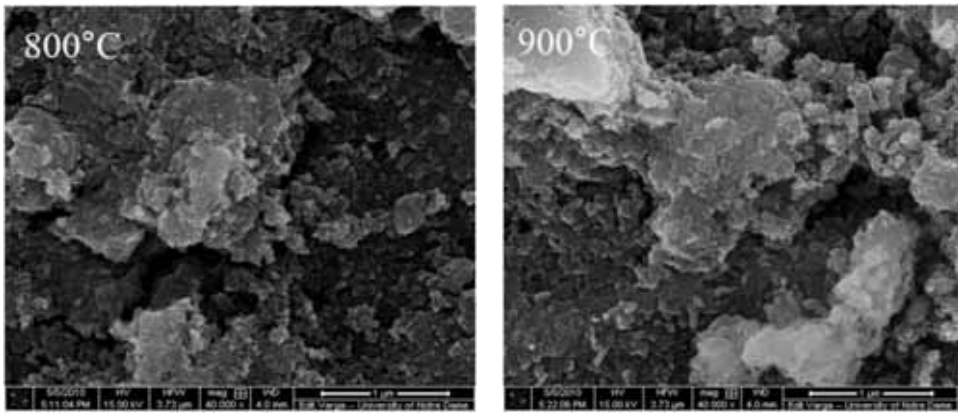

Fig. 9. SEM of heat-treated hydroxyapatite coatings.

Figure 10 illustrates a typical SEM view of cross-sections for samples heat treated under different temperatures. The multilayer coatings can be readily seen after heat treatment at 600 C (Fig. 9a), which could be due to repeated fracture. The coating layer was partially dissociated after 800°C (Fig. 9b).

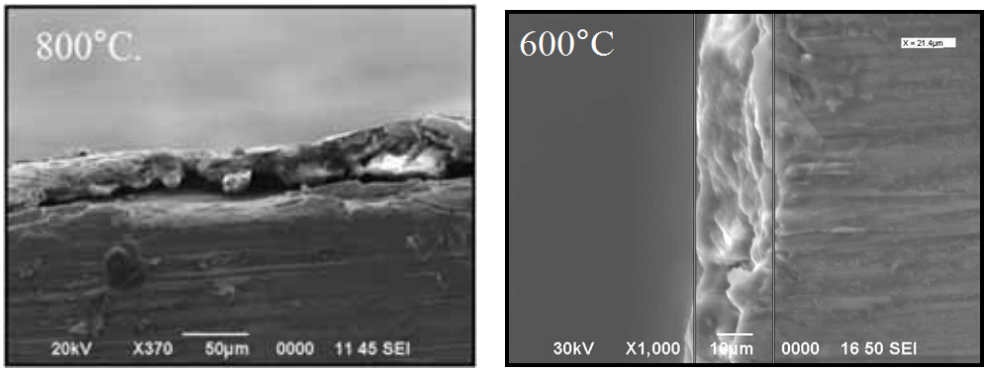

Fig. 10. Cross-section microstructure of heat-treated hydroxyapatite layer.

AFM observation of the coating (Figure 11) showed the presence of nano-sized HA. This feature could not be resolved by SEM. The high specific area generated by this topography may be associated to the high bioactivity of this coating. According to the AFM measurements, the HA range of particle sizes for the annealed sample at 700°C is 40-70 nm.

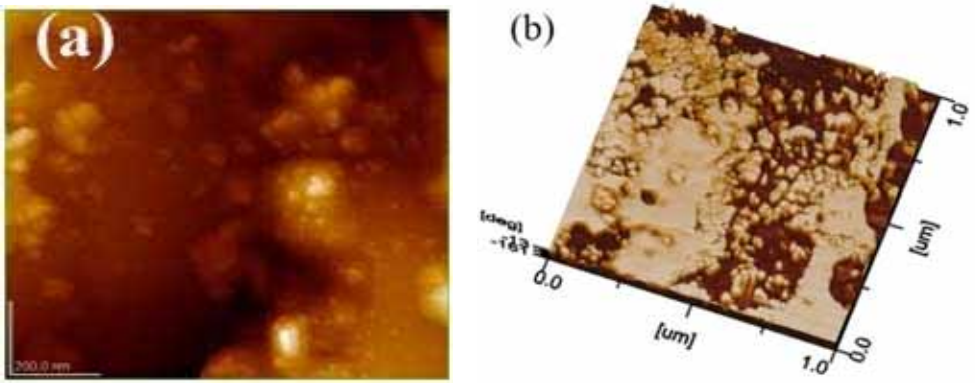

Fig. 11. Surface structure analyzed by means of AFM of heat-treatedhydroxyapatite at 700°C.
(a) Topography and (b) Phase

Titanium doped hydroxyapatite

The incorporation of Ti into the HA structure was found to inhibit grain growth without comprising the densification. In addition, the grain size decreased with increasing Ti content (0.8 and 1.6 wt.%Ti) in HA, and the number of surface grain boundaries per unit length increased, thus leading to an increase in surface activity [20]. However, only limited literature is available on the incorporation of Ti into the HA structure. Interaction of HA with titanium ions was indirectly performed at the HA–Ti interface of the HA coatings on the Ti-substrates. Mutual diffusion of elemental Ti and the ions in HA across the interface was observed which might be considered as an evidence for the incorporation of Ti into HA structure. HA modified with Ti^{4+} ions exhibited very good photocatalytic activity in oxidation and decomposition of acetaldehyde. This effect makes possible to use them in antibacterial applications. Ti ions incorporated into Ca sites in the HA lattice. Adhesion on Ti substituted HA showed an appreciable increase when compared to pure HA [21].

TEM image of Ti-doped HA powder is presented in figure 12. It can be seen that the crystals of the mechanically milled Ti-doped HA are rounded and have drop-like morphology. According to TEM results the crystallite size of the Ti-doped HA was less than 30 nm. Comparison of the Ti-doped HA sample with that of non-doped shows that the morphology changes from needle-like shaped crystals to round. TEM results of HA samples show their dependence on the effect of Ti-addition and milling. While the initial HA specimens consist of crystallites with needles and platelets -like morphology and the milled pure HA grains are needle-like, the particle shape of the Ti-doped HA is primarily spherical.

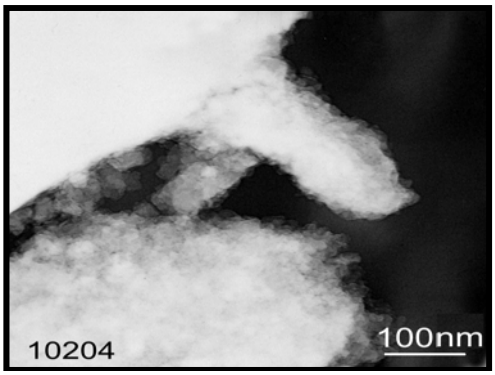

Fig. 12. Titanium-doped HA powder after one hour of mechanical alloying

The Electron paramagnetic resonance (EPR) spectrums of the HA before milling (a) with a strong peak with g-factor 2.01 and after milling (b,c) of Ti-substituted HA are shown in figure 13. The as-prepared sample heated at 350°C for 30 min. also contains signals from an ion with a g-factor of 4.23.

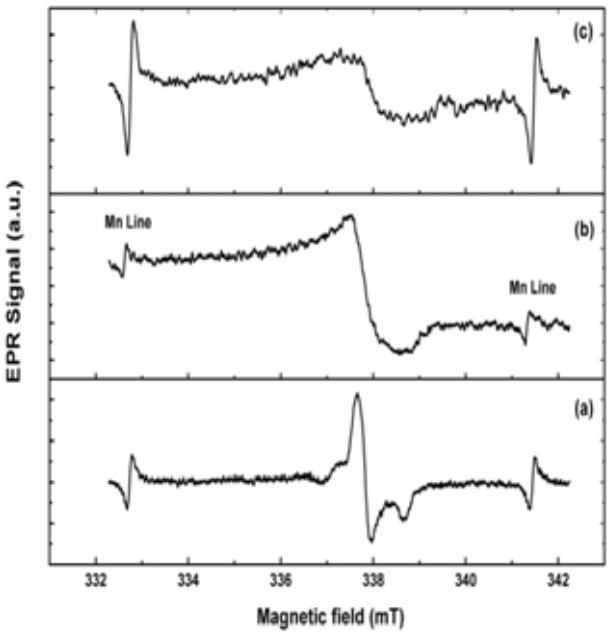

Fig. 13. R spectra of (a) hydroxyapatite powder, (b) one hour milled HA and (c) mechanical alloying Ti-doped HA.

X-Ray Diffraction Ti-doped HA coating on Ti-substrate

XRD patterns of deposited HA and 5wt.% Ti-doped HA are presented in figure 14. The changes in the XRD patterns give an indication of the influence of milling process on the structure stability of the samples. X-ray peaks of the formed phase were matched to the ICDD (JCPDS) standard, α-tricalcium phosphate (09-0348), β-tricalcium phosphate (03-0690) and titanium oxide (29-1361). XRD patterns of the HA and 5wt.%Ti-doped HA shows the Ti substrate and HA peaks. The Ti doped samples shows a notable broadening and intensity reduction comparing with pure HA after milling. The wide peaks of the deposited materials should be due to very small crystallite size.

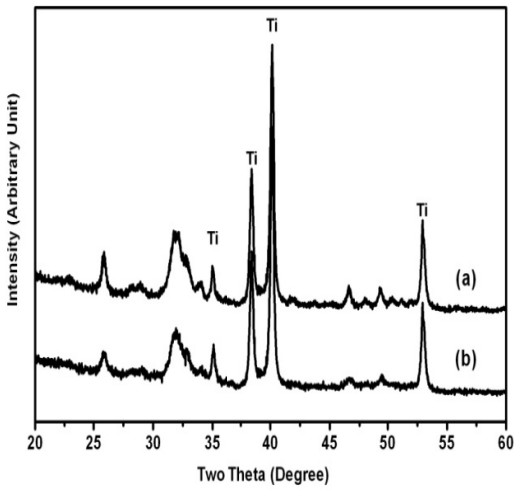

Fig. 14. XRD patterns of (a) HA and (b) 5wt.% Ti added HA coating on titanium substrate.

Morphology of Ti-doped HA coating on Ti-substrate

Backscattered electron images of the coated titanium alloy substrate surface were shown in figure 15. After one hour of milling, the substrate was partially covered with powder. The inhomogeneous distribution over the entire coated sample could be due to powder particles repeatedly fractured and cold welded on the substrate. Relatively larger covered area of the Ti-doped HA coating with respect to pure HA was seen. This could be due to Ti addition which improves the bond strength of HA.Higher magnification (3 μm) shows the particles agglomeration. Figure 15c shows cross-section microstructure of the coated Ti-doped HA. The multilayer coatings can be readily seen due to repeated fracture.

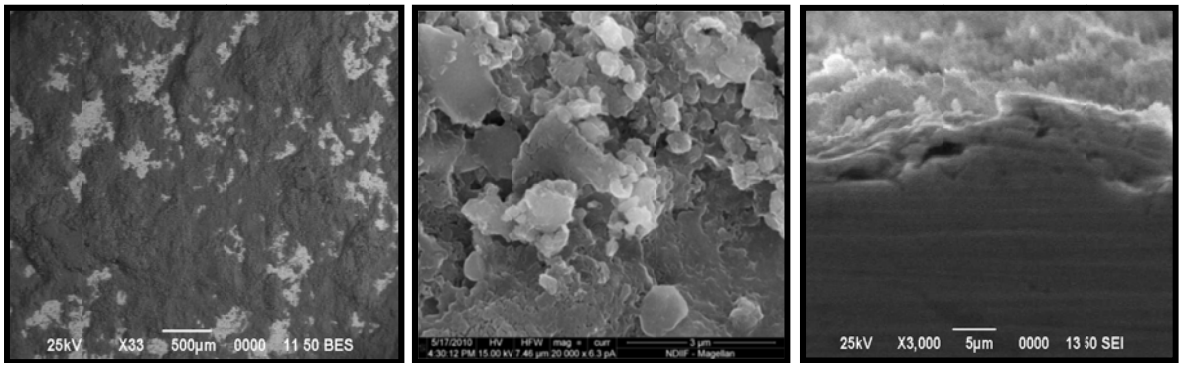

Fig. 15. Backscattered electron images of the as-synthesized 5wt.% Ti-doped HA coating after 1 h of MA (a, b) and cross-section of Ti-doped HA (c).

Diffraction heat treatment of Ti-doped HA coating

XRD patterns of deposited Ti-doped HA heated at different temperatures are presented in Figure 16. The changes in the XRD petterns provide an indication of the influence of temperature on the structure stability of the samples. X-ray peaks of the formed phase were matched to the ICDD (JCPDS) standard, α-tricalcium phosphate (09-0348), β-tricalcium phosphate (03-0690) and titanium oxide (29-1361). XRD pattern of the as-treated sample shows that, the HA after milling had wide peaks which is due to very small crystallite size formed during HEBM. Ti-doped HA samples after heat treatment up to 700°C shows that, peaks shifted slightly to higher diffraction angles due to strain release. Also according to XRD patterns, it is clear that up to 700°C of heat treatment, Ti-doped HA samples have no any indications for phase transition or decomposition. With heat treatment temperature increases the intensity of HA peaks also increases. As the heat treatment temperature reaches 800°C, the XRD patterns begin to show decomposition of the HA to $Ca_3(PO4)_2$ (TCP). The amount of TCP increases after treatment at 900°C.

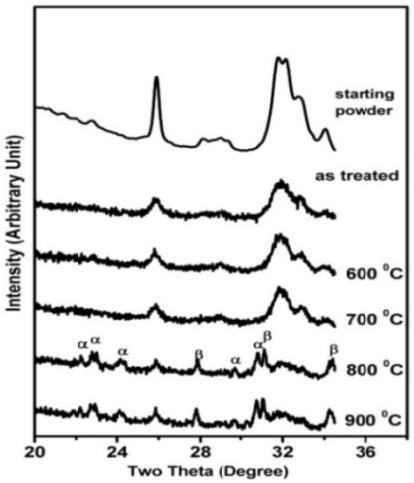

Fig. 16. XRD patterns of Ti doped HA deposited on Ti-substrate after being heated at various temperatures.

There are different proposal in the literature for possible Ti substitution mechanisms in HA structure. Among them, [21] the divalent Ca^{2+} (r_{Ca}^{2+} = 0.075 nm) cations may be substituted by quadricvalent ions of Ti^{4+} (r_{Ti}^{4+} = 0.064 nm) in Ti modified HA structure and therefore the lattice parameters and thus cell volume should decrease. Consequently, lattice disorder increases with the increase of Ti content. The induced lattice disorder may provoke microscopic stresses in HA matrix which may lower the required energy for the dehydration and respected decomposition of its structure. Therefore, the sinterability of HA compacts decreased with increasing the Ti concentration in its structure.

Morphology of the heat treatment of Ti-doped HA coating

Set of backscattered electron images shown in figure 17, indicates the microstructure evolution of the Ti-doped HA surface after various heat treatments. It can be noted that number of cracks and their width increase with increase of temperature. No other significant changes can be observed. The presence of the cracks could be due to the difference in coefficients of thermal expansion of HA and Ti-alloy substrate. The coefficient of thermal expansion (CTE) of HA is 15 x 10^{-6} K^{-1} and that of Ti is 8.6 x 10^{-6} K^{-1}.

MA is an effective way of creating localized plastic deformation, so the cracks formation after heat-treated also could be also due to mechanical energy released. The strengthening mechanism of the co-deposited HA/Ti composite coatings should relate to the dispersion strengthening by homogeneous distribution of Ti particles in the HA. It is also likely that the bonding strength of HA/Ti coating can be improved through a mechanism in which the CTE mismatch between the HA/Ti coating and the Ti substrate is reduced [22, 23].

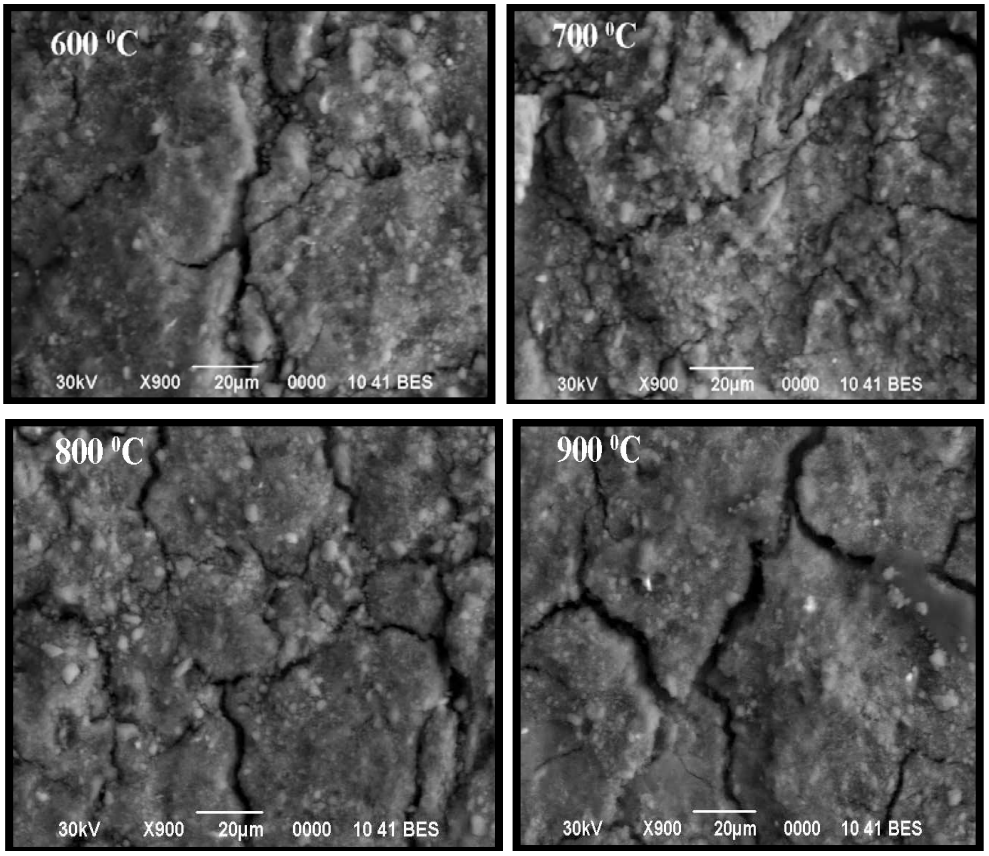

Fig. 17. Backscattered electron images of the of the heat treated Ti-doped HA coating.

Silicon doped hydroxyapatite

Recently, [24, 25] experimental work on HA and its substituted counterparts such as silicon-doped HA (SiHA) has focused on finding a measurable indicator of bioactivity. It is found that dissolution or mineralization of HA may start from dislocations and defects at the grain boundaries in dental HA. Within synthetically produced hydroxyapatite these boundaries are ‘‘clean’’ with few defects or voids. More recently a study was undertaken to investigate grain boundary structures in hydroxyapatite and silicon-substituted hydroxyapatite. It was revealed that while there was no significant difference in dislocation density between HA and Si-doped HA there was certainly an increase in triple junctions within creased silicon doping. Also it is shown that the dissolution does occur preferentially from grain boundaries and triple junctions. Additionally, at triple junctions, it was the smallest grains that showed the greatest dissolution, suggesting that a decrease in grain size would lead to increased solubility and hence greater bioactivity. It is of particular interest to note that after sintering, Si-doped HA has been shown to have a much finer grain structure than phase-pure HA suggesting that silicon inhibits grain growth. These smaller grains in Si-doped HA and the increased number of triple junctions make it an attractive candidate for enhanced bioactive products.

X-Ray Diffraction silicon doped hydroxyapatite

Figure 18 a,b shows the XRD patterns of the pure HA powder before and after milling for 1h, while figure 18 c shows such patterns for Si-doped HA powder. Significant changes were detected in the XRD patterns when after HEBM. The Si doped sample (c; see also insert in Fig.18) shows a notable broadening and intensity reduction comparing with HA powders before and after milling. In fact, the peak sharpness in XRD pattern of Si doped HA powder is lower and the peaks less resolved. The powder crystallinity strongly decreases when silicon enters into the HA structure. The same behavior was observed [26] with Si content less than 2.41 weight percent. Due to the mechanical deformation introduced into the powder and enhance Si solubility, the particle and crystallite could be refined and the lattice strain increases more than the pure HA. As seen in figure 18, the (002) reflections of the as treated HA powders containing slightly Si shifted to lower angles this could indicates that Ca^{2+}cations were substituted by Si.

The SiHA sample shows a notable broadening and intensity reduction comparing with HA. The wide peaks of the deposited materials should be due to very small crystallite size and micro-strain. Silicon has now become a major focus for research due to its critical involvement in bone growth. Concerns about crystal structure changes in the HA on incorporation of silicon have been addressed by several experimental groups. Importantly it has been found that the incorporation of silicon into the crystal has little effect on the crystal structure. X-ray diffraction studies revealed that the intensity, width and position of peaks for 0.4, 0.8 and 1.5 wt% silicon HA were very similar to those of phase-pure hydroxyapatite. Although there are no dramatic changes in the crystal structure it should be noted that increasing the silicon content of the crystal does produce a slight change in the lattice parameters. Recent experimental work has shown that there is a systematic increase in the c-lattice parameter and a concomitant increase in cell volume with increasing silicon content. It is important to recognize that the silicate has a formal charge of –4, compared to –3 for the phosphate group. In compensating for this excess negative charge it has been found experimentally that, on average, one hydroxyl group leaves the crystal for every silicon substitution [27].

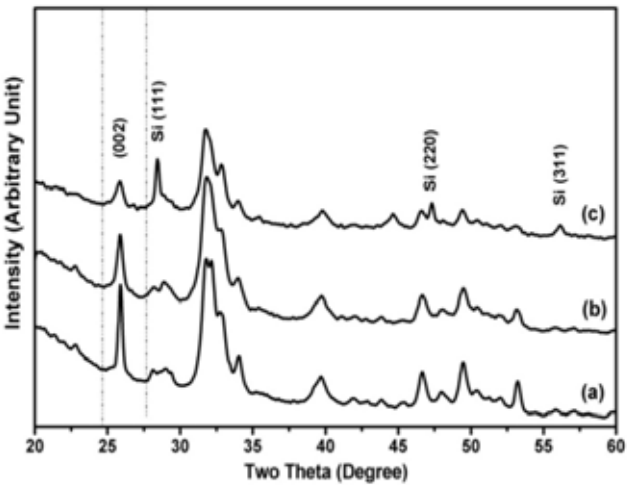

Fig. 18. XRD patterns of (a) hydroxyapatite powder, (b) milled hydroxyapatite and (c) mechanical alloying Si doped hydroxyapatite.

Morphology of silicon doped hydroxyapatite

Morphology of the Si-dope HA powder was examined using SEM and TEM. Cold welding and fracturing are the two essential processes involved in the mechanical milling/alloying process. After HEBM (W_p:W_b=1:40) the particles morphology changes due to micro-forging, fracture, agglomeration and de-agglomeration. Thus the particle becomes smaller in size due to fracturing and agglomerated by cold welding through the milling process (figure 19a). The TEM pictures of mechanically milled Si-dope HA sample are presented in figure 19b and c. It can be seen that a small round shaped crystals with size of ~ 25nm are formed during milling process.

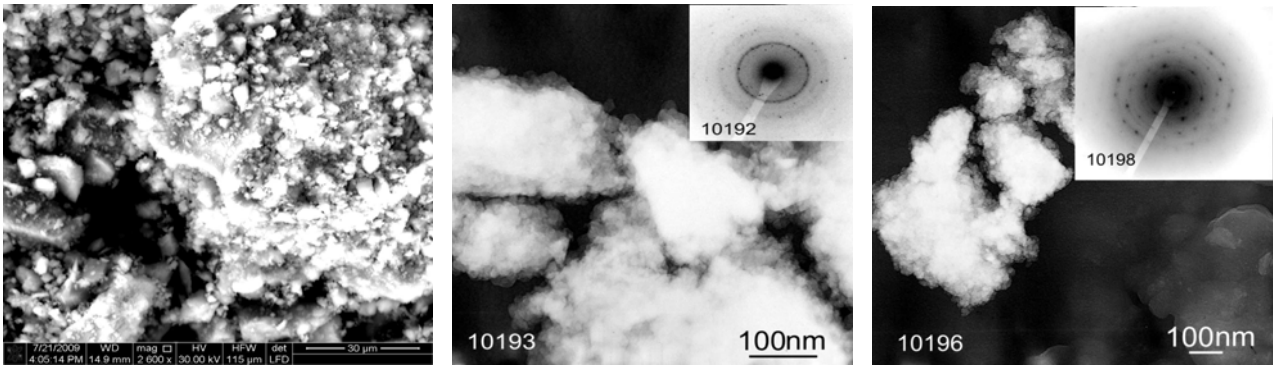

Fig. 19. SEM (a) and TEM (b,c,) images Si-doped HA after 1h of HEBM

X-Ray Diffraction of Si-doped HA Coating

XRD patterns of deposited Si-doped HA are presented in figure 20 The changes in the XRD patterns give an indication of the influence of milling process on the crystal structure of the samples. X-ray peaks of the formed phases were matched to the ICDD (JCPDS) standards. Peaks of HA, Si and Ti phases were detected.

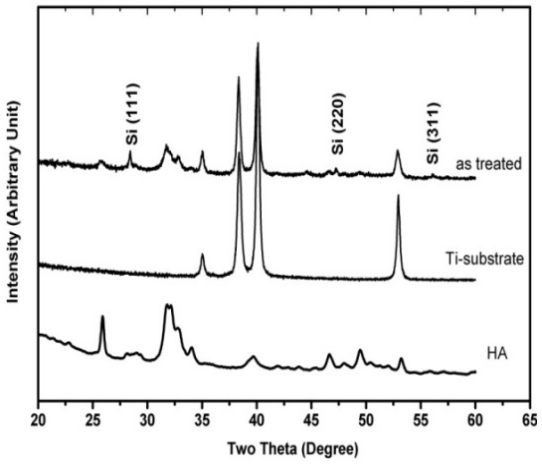

Fig. 20. XRD patterns of the SiHA coated Ti-substrate.

Morphology of Si-doped HA Coating

Backscattered electron images of the Si-doped HA surfaces coated on titanium alloy substrate are shown in figure 21. After 1hour of HEBM, the substrate was covered by HA layer in much more extent as compared to pure HA powder. This could be due to Si addition which improves the bond strength of HA. At higher magnification (Fig.21b) one can see the Ti surface deformation and HA adhesion to the substrate. Figure 21c shows the microstructure of the cross-section of the Si-dope HA coating. The composition of the along the coated sample was analyzed by energy dispersive X-ray spectroscopy (EDS). Figure 21d shows the corresponding concentration profile at the boundary between the intermixing region and the coating. It can be concluded that cold welding between particles and substrate under repeated ball collisions led to the formation of a composite coating where the HA (Ca, P, O-elements) and Si phases flowed into the pores in Ti substrate. The homogeneous distribution of Si particles in the HA formed by HEBM improves the bonding strength between coating and substrate.

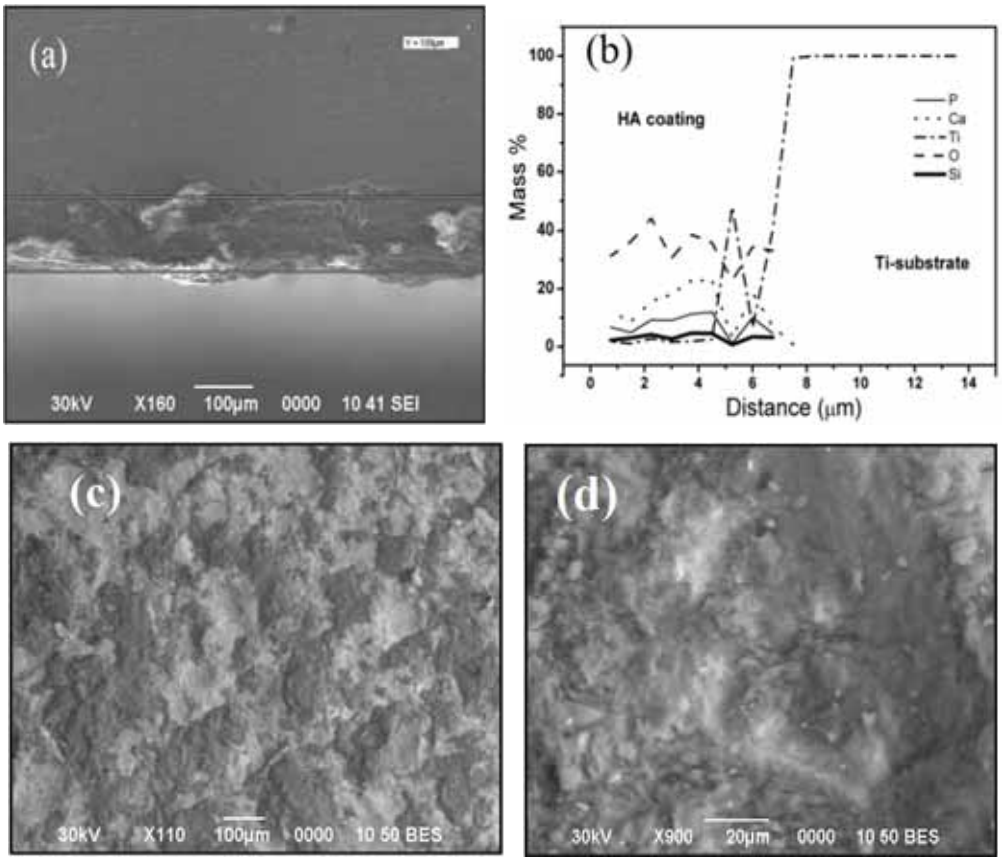

Fig. 21. Backscattered electron images of Si-doped HA coating:
(a) cross-section; (b) elements concentration profile; view from the top(c,d)

X-Ray Diffraction of heat treatment Si-doped HA coating

XRD patterns of Si-doped HA heat treated at different temperatures are presented in figure 22. The changes in the XRD patterns give an indication of the influence of temperature on the structure stability of the samples. X-ray peaks of the formed phase were matched to the ICDD (JCPDS) standard. XRD pattern of the as-treated sample shows wide peaks owing to very small size of formed crystallites. After heat treatment peaks shifted slightly to higher diffraction angles due to strain relaxation. It is important that in the whole range of heat treatment conditions (up to 900 C) Si-doped HA samples have not show phase transition or decomposition. With increasing heat treatment only the intensity of HA peaks increases compared to that of as-treated sample due to re-crystallization process.

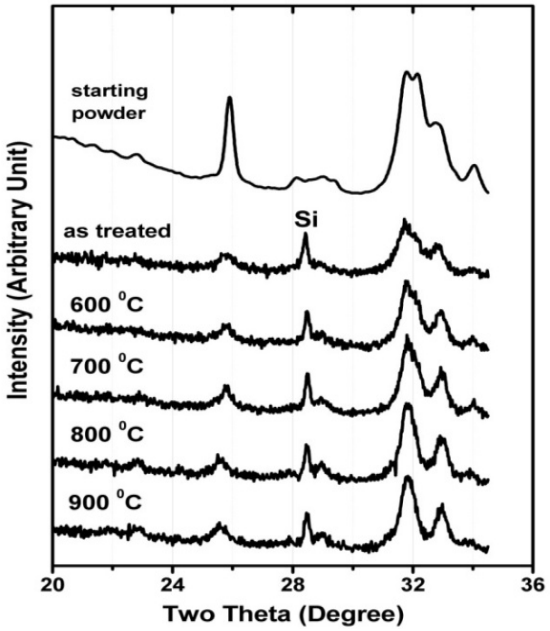

Fig. 22. XRD patterns of SiHA deposited on Ti-substrate after being heated at various temperatures.

Morphology of heat treatment Si-doped HA coating

Figure 23 shows set of backscattered electron images, indicating the microstructure evolution in the treated surface after various heat treatments. It can be noted that no any visible changes in microstructure were observed after treatment in the range of 600-800 C. The cracks are detected only after treatment at high temperature of ~ 900°C.

However, the interface between HA and a metallic implant has been another matter of concern in terms of the mechanical properties and biocompatibility of the implant. In order for the HA coating to be effective and reliable, it must be strongly bonded to the metallic surface. The analysis of cross section of heat treated Si-doped HA samples (thickness 130µ at 700°C and 55µm at 900°C) shows that the coatings possess very good adhesion to the Ti-substrates, figure 24.

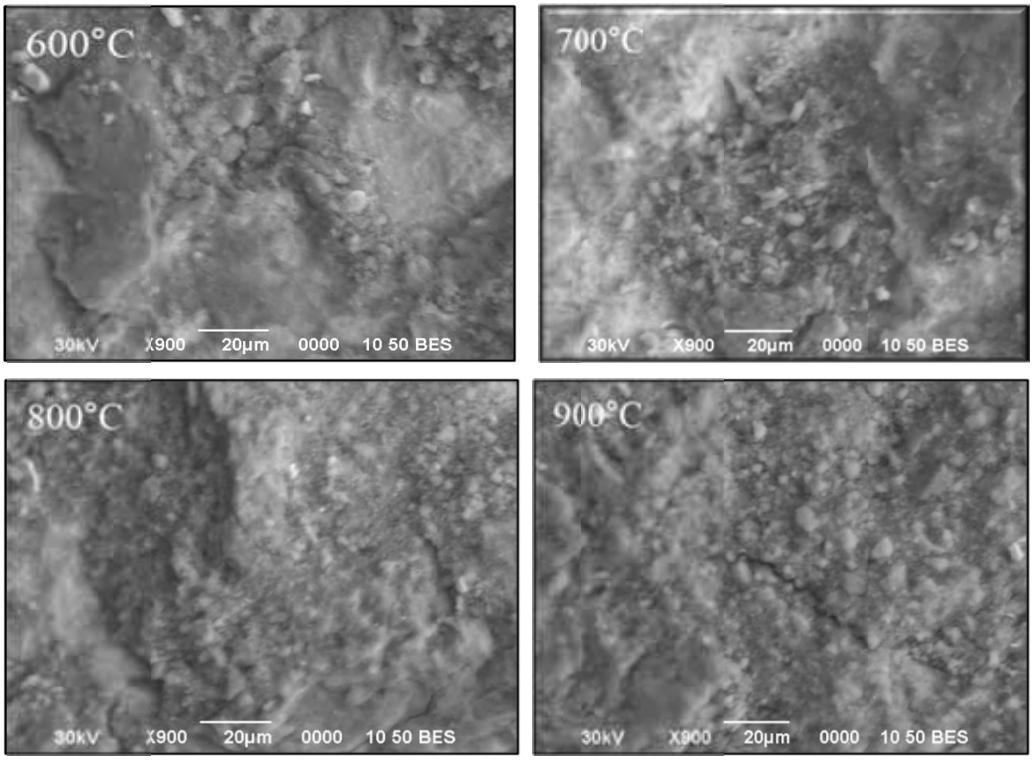

Fig. 23. Backscattered electron images of Si-doped HA coating after heat treatment under different conditions.

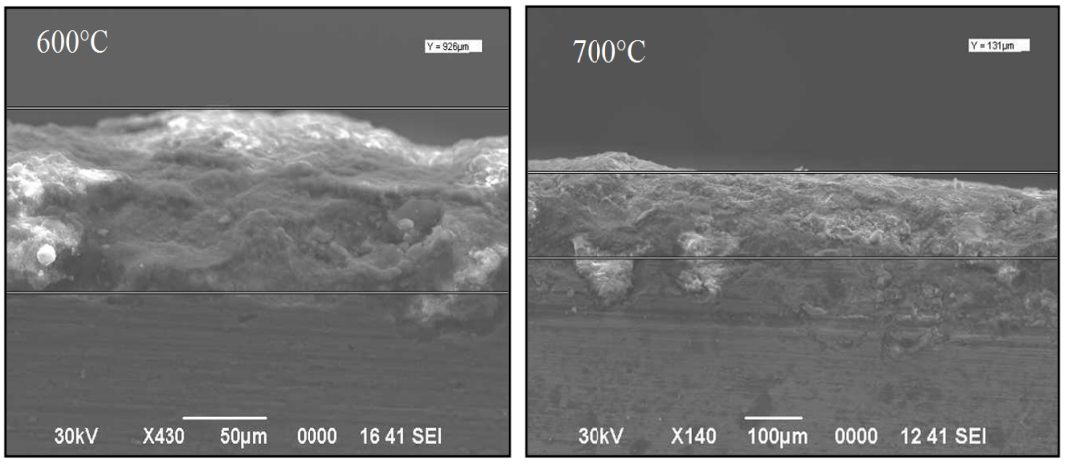

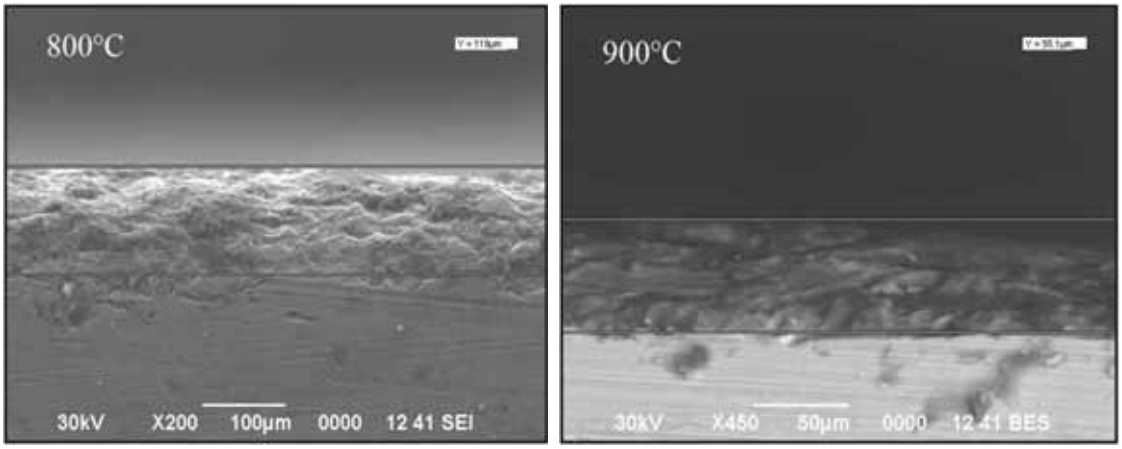

Fig. 24. Cross section of heat treated Si-doped HA samples after heat treatment under different conditions.

Amorphization Degree

The quantitative comparison, of the X-ray amorphization degree for different coatings (pure -; Ti-doped and Si-doped - HA) was made based on estimations of the intensity and background for the most intensive diffraction peaks (see Figure 25). It can be seen that XRD peaks became substantially broader after ball HEBM. Also broadening of the Si-doped sample was slightly larger than that for Ti-doped ones. The latter effect can be attributed not only to crystallite-size reduction and introduction of lattice microstrain but also to the dissolution of Ti or Si in HA lattice.

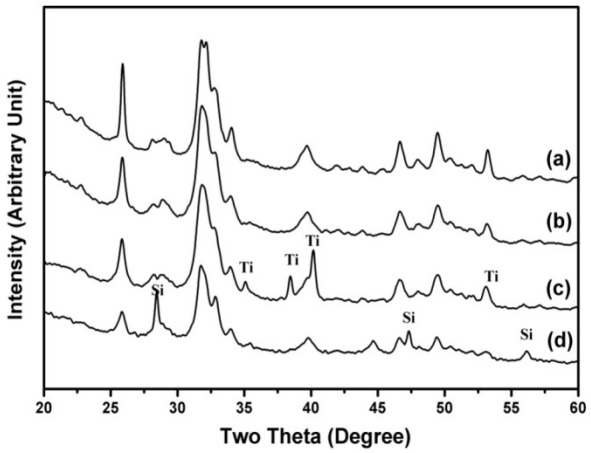

Fig. 25. XRD patterns of coated (a) HA, (b) as-milled, (c) TiHA and (d) SiHA milled for one hour

Conclusion

Thus based on the detailed studies of using the high energy ball milling technique for depositing of ceramic coating on the metal substrate a novel approach for production of hydroxyapatite (HA) films on titanium substrates has been developed. During HEBM process the impacts of the milling balls activate the metal surface and lead to the robust cold-welding of HA particles to the metal surface. It was shown that HEBM also results in significant decrease of the HA particle and crystalline size, forming the nano-scale structure. It was demonstrated that a heat treatment of the mechanically coated HA at 800°C for one hour leads to partial transformation of HA phase to β-TCP. It appears that the grain boundary and interface defects formed during HEBM reduce the transformation temperature. Also, it was shown that Ti incorporation into the HA structure causes the lattice shrinkage and reduction of its grain size as compared to pure HA, but also promote the phase transformation of HA to TCP during heat treatment. It is important that doping HA by silicon, while also significantly decrease the crystal size of HA layer, results in hindering of the phase transformation process. The Si-doped HA does not show phase transition or decomposition after heat treatment even at 900 °C.

References

1. Johnson S., Haluska M., Narayan R.J., Snyder R.L., *Materials Science and Engineering C*, 26:1312(2006).
2. Albayrak O., El-Atwani O., Altintas S., *Surface & Coatings Technology*, 202,11:2482(2008).
3. Khor K.A., Yip C.S., Cheang P., *Journal of Thermal Spray Technology*, 6(I):109(1997).
4. Wang C.K., Chern Lin J.H., Ju C.P., Ong

H.C., Chang R.P.H., *Biomaterials*, 18:1331(1997).
5. Xiao Y., Li D., Fan H., Li X., Gu Z., Zhang X., *Materials Letters*, 61:59 (2007).
6. Shih W.J., Chen Y.F., Wang M.C., Hon M.H., *Journal of Crystal Growth* , 270:211(2004).
7. Hannora A., Mamaeva A., Mansurov Z., Surface Review and Letters, 16,5:781(2009).
8. Hannora A., A. Mamaeva, N. Mofa, S. Aknazarov, Z. Mansurov, Eurasian Chemico-Technological Journal, 11, 1:37(2009).
9. Shih W.J., Wang J.W., Wang M.C., Hon M.H., *Materials Science and Engineering C*, 26:1434(2006).
10. SuryanarayanaC. Mechanical alloying and milling. *Progress in Materials Science*, 46 (2001), 1-184.
11. El-Eskandarany M., Aoki K., Itoh H., Suzuki K.., *Journal of the Less Common Metals*, 169:235(1991).
12. Krupa D., Baszkiewicz J., Kozubowski A., Lewandowska-Szumieł M., Barcz A., Sobczak W., Bilinski A. and Rajchel A., *Bio-Medical Materials and Engineering*, 14:525 (2004).
13. Dıaz-Estrada J. R., Camps E., Escobar-Alarcon L. Ascencio J. A., *J. Mater. Sci.*, 42:1360(2007).
14. White T., Ferraris C., Kim J., Madhavi S., *Reviews in Mineralogy & Geochemistry*, 57:307(2005).
15. Ramesha S., Tan C.Y., Sopyan I., Hamdi M., Teng W.D., *Science and Technology of Advanced Materials*, 8:124(2007).
16. Mayer I., Cuisinier G., Gdalya S., PopovI., *Journal of Inorganic Biochemistry*, 102:311 (2008).
17. Ribeiroa C., Gibsond I., Barbosa M. The uptake of titanium ions by hydroxyapatite particles-structural changes and possible mechanisms. *Biomaterials*, 27 (2006), 1749–1761.
18. Zhang D.L., *Progress in Materials Science*, 49:537(2004).
19. Mahe M., Heintz J., Rodel J., Reynders P., *Journal of the European Ceramic Society*, 28:2003 (2008).
20. Huang J., Best S.M., Bonfield W., Buckland T., *Acta Biomaterialia* (2009), In Press.
21. ErgunC., *Journal of the European Ceramic Society*, 28:2137(2008).
22. Xiao X.F., Liu R.F., Zheng Y.Z., *Materials Letters*, 59:1660(2005).
23. Ergun C., Doremus R.. *Turkish J. Eng. Env. Sci.*, 27:423(2003).
24. Lopez-A lvarez M., Solla E. L., Gonzalez P., Serra J., Leon B., Marques A. P., Reis R. L., *J Mater Sci: Mater Med*, 20:1131(2009).
25. Zou S., Huang J., Best S., Bonfield W., Journal of Materials Science: Materials in Medicine, 16:1143(2005).
26. Sprio S., Tampieri A., Landi E., Sandri M., Martorana S., Celotti G., Logroscino G., *Materials Science and* Engineering C, 28:179(2008).
27. Chappell H.F., BristoweP.D., J Mater Sci: Mater Me*d*, 18:829(2007).

Received 8 September 2009.